

Six-Port Radar Sensor for Remote Respiration Rate and Heartbeat Vital-Sign Monitoring

Gabor Vinci, *Student Member, IEEE*, Stefan Lindner, *Student Member, IEEE*,
 Francesco Barbon, *Student Member, IEEE*, Sebastian Mann, *Student Member, IEEE*,
 Maximilian Hofmann, *Student Member, IEEE*, Alexander Duda, Robert Weigel, *Fellow, IEEE*, and
 Alexander Koelpin, *Member, IEEE*

Abstract—A novel remote respiration and heartbeat monitoring sensor is presented. The device is a monostatic radar based on a six-port interferometer operating a continuous-wave signal at 24 GHz and a radiated power of less than 3 μ W. Minor mechanical movements of the patient's body caused by the respiration as well as heartbeat can be tracked by analyzing the phase modulation of the backscattered signal by means of microwave interferometry with the six-port network. High-distance measurement accuracy in the micrometer scale as well as low system complexity are the benefits of the six-port receiver. To verify the performance of the system, different body areas have been observed by the six-port radar. The proposed system has been tested and validated by measurement results.

Index Terms—Heartbeat monitoring, remote sensing, respiration rate monitoring, six-port, vital sign.

I. INTRODUCTION

HEARTBEAT and breath rate monitoring is of primary interest for several medical applications that range from simple vital-sign detection to accurate monitoring of a patient's health status. Several different diagnosis procedures benefit from these vital-sign monitoring techniques. For instance, the ability to observe the breath and heartbeat of a patient overnight allows one to detect sleep disorders or anomalies. Another promising approach could be the early and contactless detection of Sudden Infant Death Syndrome (SIDS), which is still the leading cause of infant death, accounting for approximately 25% of all deaths of children younger than one year of age [1], [2]. Further, the workaday life in clinical environments could benefit from such a system, since a patient will not have to be connected by wires in order to be monitored. Within the next several years, the market of cardiovascular monitoring and diagnostic (CMD) devices such as electro-cardio-graph (ECG) or cardiopulmonary diagnostic devices (CPDs) is expected to reach over one billion USD with a 5% annual growth rate [3], to a wide diffusion of such monitoring devices not only in hospitals and medical care centers but also in domestic environments for homecare and telemedicine. For these kinds

of scenarios, contactless ECG and CPD techniques are strongly preferred and have therefore been of great interest lately in the medical and scientific community.

II. STATE OF THE ART

Several different concepts based on different physical principles have been proposed, although most of the introduced contactless concepts are based on the detection of minor geometrical changes of the patient's torso due to heartbeat and breathing. In order to detect such minor variations, several solutions based on the radar principle with traditional heterodyne transceivers were introduced in the past [4]. First Doppler radar experiments were conducted in the early 1970s, nevertheless, poor performance of the proposed approaches led to the introduction of alternative systems [5]. Those are based on pneumatic mattress sensors or carbon dioxide detectors for breath monitoring; however, these techniques can only be considered as semicontactless [6], [7]. Thus, radar techniques are preferred due to several advantages with respect to other solutions. An improvement in performance of various radar techniques in the last decade boosted the research oriented towards this particular application scenario [8]–[11]. Several approaches based on frequency-modulated continuous-wave (FMCW) radar techniques attracted the attention of the scientific community. However, only a few radar systems that have been presented reach the required accuracy. Most FMCW radars require an extremely wide frequency band of operation to reach the required accuracy level. Some advanced FMCW systems perform measurements with an accuracy in the micrometer range [12]. Though the performance of such systems is strongly related to the linearity of the generated frequency ramps. Nonidealities in the frequency sweep from the voltage-controlled oscillator (VCO) of the FMCW radar device introduce measurement errors. Furthermore, another relevant aspect for the right choice of the frequency of operation is the spectrum allocation with different bands and licensing schemes. For the target applications, it is necessary that a radar based sensor works within specified Industrial-Scientific-Medical bands (ISM). Therefore, such devices always need to satisfy a trade off between bandwidth, compliance within ISM bands and center frequency of operation. Other alternative radar techniques that satisfy these criteria have also been introduced. Continuous Wave (CW) radar technology has been implemented showing excellent results [13]. Nevertheless, most accurate measurements of minor distance variations can be performed by interferometric methods. Lately, a lot of

Manuscript received October 15, 2012; revised January 19, 2013; accepted January 28, 2013. Date of publication March 07, 2013; date of current version May 02, 2013.

The authors are with the Department for Electronics Engineering, University of Erlangen-Nuremberg, 91058 Erlangen, Germany (e-mail: gabor.vinci@ieee.org).

Color versions of one or more of the figures in this paper are available online at <http://ieeexplore.ieee.org>.

Digital Object Identifier 10.1109/TMTT.2013.2247055

research has been conducted on alternative microwave interferometric radar techniques. Microwave interferometry offers the advantages of microwave propagation and material interaction with high resolution and low complexity of the radar device. The six-port receiver architecture, used as an interferometer, has recently gained relevance for extremely accurate angle, displacement and vibration measurements [14]–[22]. Although well known since the early 1970s, the six-port technique gained relevance only recently in radar measurements. In comparison with the FMCW technique, instead of evaluating the frequency offset of an FMCW ramp, only the phase difference between the reference and the backscattered microwave signals is measured. The six-port interferometer can easily discriminate a phase difference in the range of $\lambda/30000$ directly at the microwave frequency, therefore, presenting excellent spatial detection accuracy. The heartbeat and breathing activities affect the phase of the reflected signal, which is compared with the reference signal source in the radar device.

III. SIX-PORT NETWORK

Introduced in the 1970s by Engen and Hoer [23] for power measurement applications, the six-port structure is nowadays known as an alternative receiver setup for microwave and millimeter-wave frequencies [24], [25]. Independent of the design, a six-port receiver is a passive structure featuring two input ports and four output ports [26]. As the six-port receiver is based on the interferometric principle, the two input signals are superimposed with each other under four different relative phase shifts. Depending on phase difference and amplitudes of the two input signals, constructive and destructive interaction takes place at the four output ports. For a six-port receiver (Fig. 1), two complex input signals \underline{P}_1 and \underline{P}_2 with carrier frequency f can be defined as

$$\underline{P}_1 = A_1 \cdot e^{j(2\pi ft + \phi_1)} \quad (1)$$

$$\underline{P}_2 = A_2 \cdot e^{j(2\pi ft + \phi_2)}. \quad (2)$$

Considering the relative phase differences between P_1 and P_2 of 0 , $\pi/2$, π , and $3\pi/2$ at the output ports, the complex output signals \underline{P}_3 , \underline{P}_4 , \underline{P}_5 , and \underline{P}_6 can be calculated as

$$\underline{P}_3 = 0.5(\underline{P}_1 + j\underline{P}_2) \quad (3)$$

$$\underline{P}_4 = 0.5(j\underline{P}_1 + \underline{P}_2) \quad (4)$$

$$\underline{P}_5 = 0.5(j\underline{P}_1 + j\underline{P}_2) \quad (5)$$

$$\underline{P}_6 = 0.5(\underline{P}_1 - \underline{P}_2). \quad (6)$$

Downconversion to baseband by power detectors (value squared) delivers the following baseband voltages B_3 to B_6 :

$$B_3 = |\underline{P}_3|^2 = 0.25|\underline{P}_1 + j\underline{P}_2|^2 \quad (7)$$

$$B_4 = |\underline{P}_4|^2 = 0.25|j\underline{P}_1 + \underline{P}_2|^2 \quad (8)$$

$$B_5 = |\underline{P}_5|^2 = 0.25|j\underline{P}_1 + j\underline{P}_2|^2 \quad (9)$$

$$B_6 = |\underline{P}_6|^2 = 0.25|\underline{P}_1 - \underline{P}_2|^2. \quad (10)$$

Due to the fact that the relative phase shifts between the four output ports are multiples of $\pi/2$,

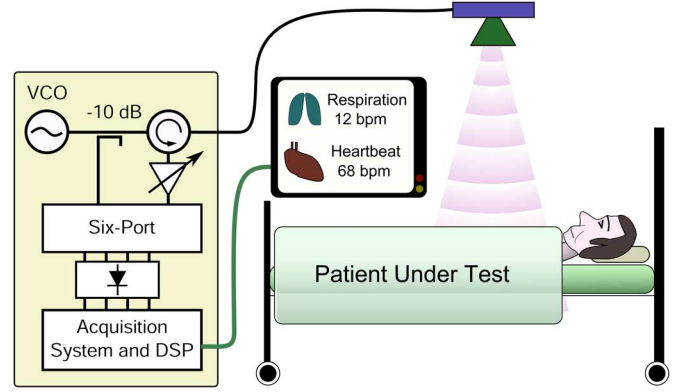


Fig. 1. System concept of the proposed sensor device.

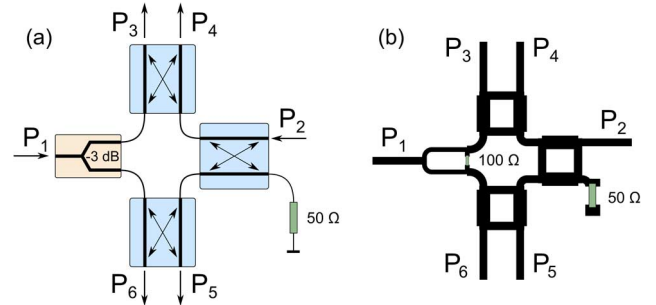


Fig. 2. (a) Circuit schematic and (b) implementation in microstrip technology of the six-port network.

there is a complex representation \underline{Z} for the baseband signals. The in-phase as well as the quadrature component each can be split up in two pairs with a relative phase shift of π in between. As a result, the baseband signals B_3 to B_6 can be handled like differential I/Q signals as

$$\underline{Z} = I + jQ = (B_5 - B_6) + j(B_3 - B_4). \quad (11)$$

Calculating the argument of the complex expression \underline{Z} leads to $\Delta\sigma$, which is equal to the phase shift between the two input signals of the six-port as

$$\Delta\sigma = \phi_1 - \phi_2 = \arg\{\underline{Z}\}. \quad (12)$$

As mentioned before, a six-port structure provides altogether two input and four output ports. Fig. 2 shows the circuit schematic and the microstrip implementation of the developed network. A Wilkinson divider and three hybrid branchline couplers generate the mentioned phaseshifts. The microstrip structure is fabricated on a $200\text{-}\mu\text{m}$ -thick Rogers RO4003 high-frequency laminate.

IV. SIX-PORT RADAR

To measure minor movements of the persons chest due to breathing and heart activity, a continuous-wave (CW) monostatic radar with interferometric evaluation is proposed. The radar is based on the six-port receiver network to perform a relative phase measurement between the received signal from the antenna and a reference signal derived through a -10dB

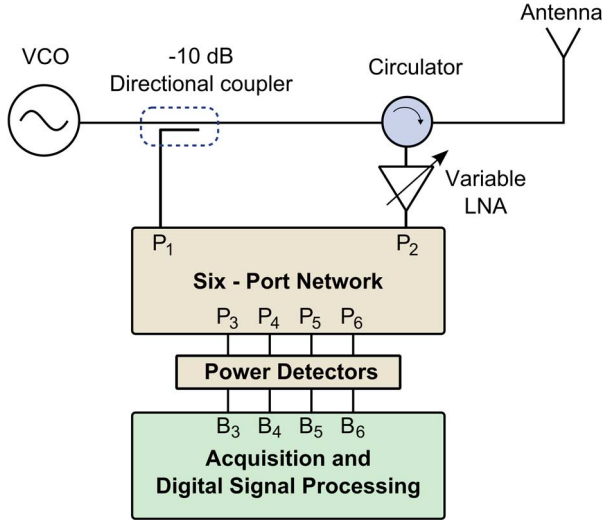


Fig. 3. Schematic of the proposed six-port based monostatic radar.

directional coupler from a microwave VCO source generating a 24-GHz CW signal (Fig. 3). The RX and TX paths are separated through a circulator installed directly behind the radar antenna. In this case, a 20-dBi gain rectangular horn antenna has been used. The received signal is amplified by a low-noise amplifier (LNA) (HMC751LC4 from Hittite) and a variable attenuator chain (Hittite HMC812LC4) to guarantee that the amplitude of the input signal P_2 at the second port of the six-port receiver is comparable to the amplitude of the reference signal P_1 at the first input port. This will ensure maximum phase resolution. The detector output signals in baseband B_3 , B_4 , B_5 , and B_6 are consequently amplified by precision low-noise operational amplifiers (LMP7718 from Texas Instruments) with variable gain configuration for signal conditioning purposes.

V. REMOTE VITAL-SIGN MONITORING

The introduced system will illuminate the patient-under-test (PUT) with an electromagnetic wave. From animal experiments, the permittivity of the upper skin layer was obtained to $\epsilon_{r,skin} = 13.6 + j10.2$ at 24 GHz. Thus, the penetration depth of the signal is determined to be 1.52 mm, which can be calculated according to

$$d_{Skin} = \frac{c_0}{2\pi f \sqrt{\epsilon'_r}} \sqrt{\frac{2}{\sqrt{1 + \left(\frac{\epsilon''_r}{\epsilon'_r}\right)^2} - 1}}. \quad (13)$$

Furthermore, the maximum reflectivity R_{Skin} of the considered tissue has been determined to be 39%, which can be calculated according to (14) and (15), while ϵ' and ϵ'' refer to the real and imaginary part of the tissue permittivity [27]:

$$\underline{n}_{Skin} = \sqrt{\frac{\sqrt{\epsilon'^2_r + \epsilon''^2_r} + \epsilon'_r}{2}} + j \sqrt{\frac{\sqrt{\epsilon'^2_r + \epsilon''^2_r} - \epsilon'_r}{2}} \quad (14)$$

$$R_{Skin} \leq \left| \frac{1 - \underline{n}_{Skin}}{1 + \underline{n}_{Skin}} \right|^2. \quad (15)$$

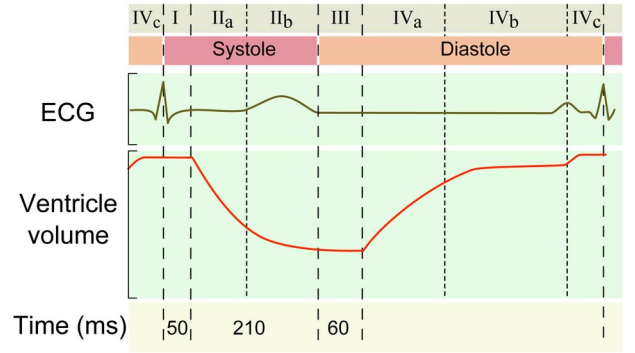


Fig. 4. Physiological explanation of the thorax movements and vibrations [28].

Since the permittivity of a blanket or clothes $\epsilon_{r,cotton} \approx 1$ is significantly smaller than $\epsilon_{r,skin}$, the radiated signal will mainly be reflected at the patient's upper skin layer. The patient's respiration will result in a significant and periodic extension of the torso, which is in the range of several millimeters. Additionally, the heartbeat will be superimposed to this movement, which is assumed to be in the submillimeter range. From Fig. 4 this correlation can be obtained. The cardiac electrical impulse is followed by a contraction of the heart muscle. Subsequently, a variation of the ventricle volume occurs which is also audible via a stethoscope for instance. The acoustic wave propagates through the thorax and leads, together with the extension of the blood vessels due to the heart expansion, to minor skin movements in the submillimeter range. This periodic movements and vibrations can subsequently be detected by extensive signal postprocessing.

VI. SIGNAL ACQUISITION AND CONDITIONING

In the proposed radar system, the four microwave output signals P_3 , P_4 , P_5 , and P_6 of the six-port interferometer structure are converted into baseband voltages by diode-based power detectors [29]. The detector structure (shown in Fig. 5) is based on an input-matching network, a gallium–arsenide zero-bias Schottky diode (Aeroflex Metelics MZBD-9161) and an output low-pass filter.

Dynamic range measurements [30] show that the proposed detector structure works for input signals from -55 dBm (tangential signal sensitivity) up to $+10$ dBm and features a voltage sensitivity of 2000 mV/mW at -40 dBm at 24 GHz [31]. The four baseband signals B_3 , B_4 , B_5 , and B_6 are sent to an antialiasing filter and then to an analog-to-digital converter (ADC) (Maxim MAX1305ECM). The acquisition system has been designed to acquire signals with an analog bandwidth up to 50 kHz featuring eighth-order Butterworth low-pass filter to avoid aliasing [30]. The signals are then sampled with 12-b resolution at 640 Ksps. A digital signal-processing board (Altera DE2) based on the Altera Cyclone2 FPGA has been used to control the signal acquisition and the signal conditioning as well as to stream the acquired raw data via Ethernet to a computer. The transmitted data is received with a dedicated software socket and then processed via MATLAB. To guarantee optimal power–voltage conversion input signals conditioning has been included, a variable RF amplification stage on the P_2

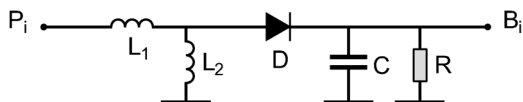
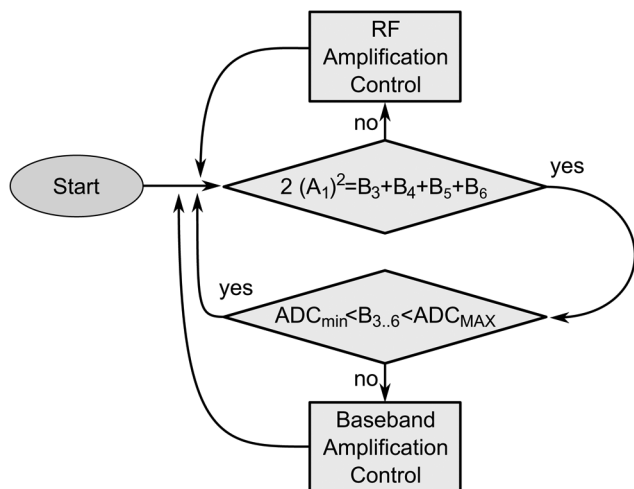
Fig. 5. Power detector network with $i \in \{3, 4, 5, 6\}$.

Fig. 6. Flowchart of the signal conditioning algorithm.

six-port input branch and baseband variable amplifiers after each power detector is used. The control algorithm (see Fig. 6) monitors the four baseband signals (B_3, B_4, B_5, B_6) acquired by the ADCs. The first condition is to guarantee the same amplitude of the two six-port input signals. This is done by changing the RF amplification of the P_2 signal. The amplitude of the reference signal (A_1) can be computed by measuring the four output voltages when the second input branch (P_2) is isolated (no received signal, $A_2 = 0$) with the following:

$$A_1 = \sqrt{B_3 + B_4 + B_5 + B_6}|_{A_2=0}. \quad (16)$$

When this first condition is satisfied, a second conditioning step based on the control of the baseband amplifiers will be executed. Independent amplifiers are used to fit the baseband signals (B_3, B_4, B_5 , and B_6) to the ADCs input dynamic range.

The conditioning algorithm works in real time in order to avoid any possible signal saturation and to guarantee the best acquisition condition.

VII. DIGITAL SIGNAL PROCESSING

To obtain the heart beat and respiration rate, it is necessary to perform several digital signal-processing steps. At first, a simple calibration algorithm is used to remove offset and gain errors caused by the analog to digital conversion. After that, the desired signal frequencies have to be filtered and the rates calculated. The whole signal processing is done by MATLAB, which is also used to received the streamed data from the measurement setup.

A. Initial Calibration

An initial calibration has to be done, because of the imperfections of the realized six-port microstrip circuit, diode detector nonidealities as well as imperfections of the analog baseband signal conditioning. The result of these influences can be seen

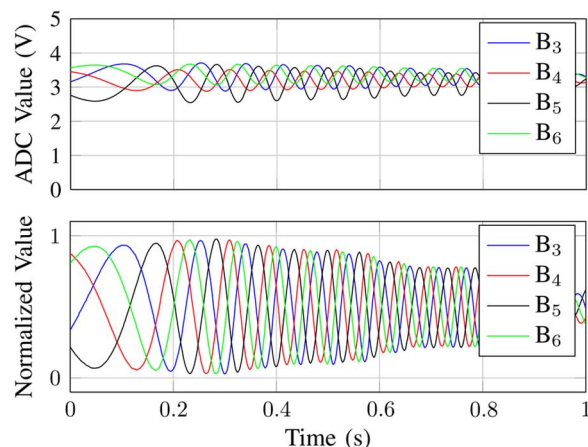


Fig. 7. Digitized raw six-port output voltages with offset and gain errors together with the compensated signals.

in the top of Fig. 7 as an obvious gain and offset mismatch between the four six-port output channels.

To compensate for these errors, the acquired signals must sweep the entire dynamic range to detect offset and gain errors. To do this, the body of the PUT has to move one time more than a half wavelength of the used RF. In this use case, this means a movement of more than $1/2\lambda_{RF} = (c_0/2 \cdot f_{RF}) \approx 6$ mm. With the acquired information, the maximum amplitudes of the single channels can be measured and therefore offset and gain can be corrected. This condition is easily satisfied when the PUT is observed by the monitoring system for several seconds before starting the measurement. Within this initial observation time window, a calibration can be performed as soon as the person inhales and exhales one time.

Further compensation is not necessary for this measurement setup because only relative changes in the distance are evaluated to calculate the heartbeat and respiration rate.

B. Six-Port Specific Signal Processing

The vital parameter monitoring is based on a continuous measurement of the distance between the radar module and the PUT. This distance information can be extracted from the baseband voltages by considering (11) and (12) through equation

$$d = \frac{1}{2} \cdot \frac{\Delta\sigma}{2\pi} \lambda_{RF}. \quad (17)$$

This equation describes the projection of the phase difference between transmitted and reflected signals to the used wavelength leading to a distance. The correction factor of $1/2$ is caused by the round trip from the radar module to the PUT and back that the wave has to travel. It is obvious that this distance calculation leads to an ambiguous distance measurement if the target moves more than half of a wavelength. However, because of the continuous monitoring, the appearing phase wraps can easily be detected and corrected by commonly known phase unwrap algorithms.

C. Digital Filtering and Vital Parameter Extraction

To reduce the noise and select only the needed frequencies of respiration rate and heartbeat, the calculated distance signal is digitally filtered. Therefore, a fifth-order low-pass filter with a

TABLE I
MEASURED RF POWER LEVELS AND EIRP VALUES

	VCO	antenna feed	EIRP
in dBm	-22.2	-25.6	-5.6
in μ W	6	2.75	275

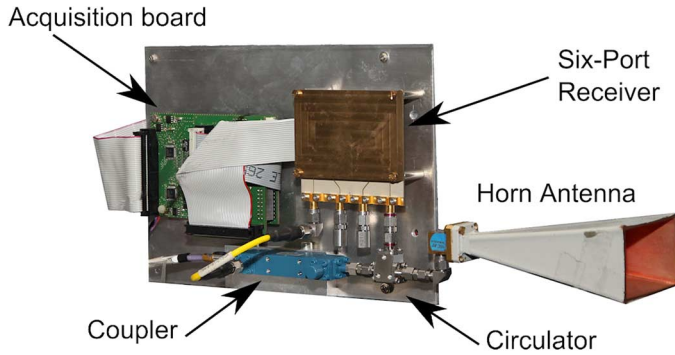


Fig. 8. Photograph of the hardware prototype.

cutoff frequency of 200 bpm (3.33 Hz) and Butterworth characteristic is implemented to remove high-frequency noise signals. This filtering does not influence the respiration rate or heartbeat rate in the range of 0 bpm (lowest possibility for breathing) up to 180 bpm (upper limit for heart rate).

The cutoff frequency of the second filter stage is adjustable and depends on the detected breathing frequency. The frequency is chosen to be slightly over the first harmonic of the detected breathing frequency, which is calculated by peak detection in the power spectral density (PSD) spectrum of the low-pass-filtered signal. The PSD is evaluated by a fast Fourier transformation (FFT).

With the calculated filter coefficients for the second high-pass filter stage, the previously filtered distance signal can be band-limited to the signal frequencies of the heartbeat rate. This heartbeat rate can now be detected with a peak detection in the resulting PSD.

VIII. MEASUREMENT RESULTS

A. Emitted Power Levels

To ensure the patient's safety, especially under monitoring conditions (this means continuous observation with the CW radar), the radiated power levels have to be considered. Therefore, measurements were done with a thermal power sensor (Rohde & Schwarz NRP-Z55) to measure the actual power levels in the system. The measurement results are shown in Table I, where the measured output power of the used VCO and the power level at the antenna feed are shown. The equivalent isotropic radiated power (EIRP) is calculated using the antenna feed power and the gain of the used 20-dBi horn antenna.

B. Vital Parameters

A standard measurement has been performed with the PUT lying on his back as the six-port based radar sensor was observing the chest of the PUT at a distance of approximately 1 m. A photograph of the complete radar sensor is shown in Fig. 8. The results are plotted in Fig. 9. In the raw time-domain data of

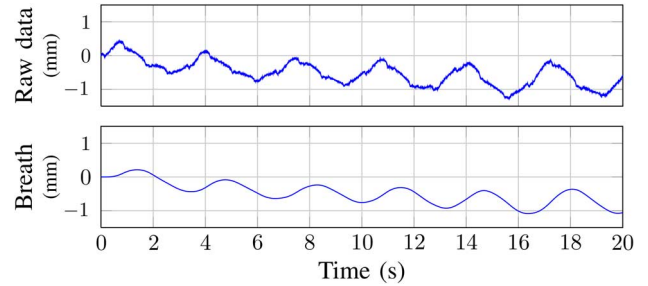


Fig. 9. Time-domain signal of the measured raw data and low-pass-filtered breathing signal. The signal delay in the respiration signal is due to the response of the introduced filter.

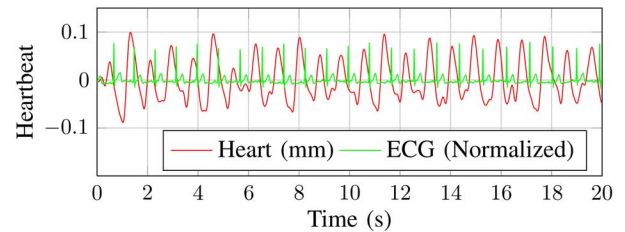


Fig. 10. Measured heart beat signal in the time domain compared with a reference ECG.

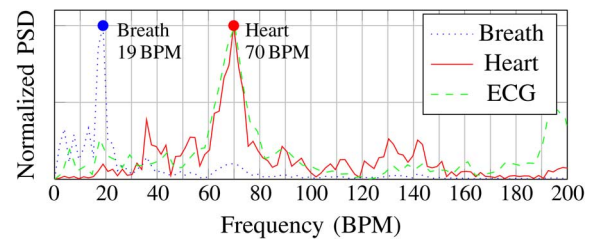


Fig. 11. Normalized PSD of the measured breath and heart-rate signals compared with the PSD of a reference ECG.

the modulated distance, it is possible to recognize the breathing as well as minor heart activity. By properly filtering the raw signal, a clear time-domain respiration monitoring can be performed (Fig. 9). Subtracting the calculated respiration signal from the raw data, it is possible to extract the heartbeat signal, which is plotted in Fig. 10. Please note that no hard synchronization of ECG and radar-based heart signal has been applied due to the influences of the filter response in the time domain.

For a direct comparison, the detected heartbeat signal is compared with a reference ECG from a dedicated ECG measurement belt. The measurement match exactly the reference ECG signal. Furthermore, a frequency-domain analysis has been performed. The PSD of the signal has been calculated with an FFT leading to the results plotted in Fig. 11. A peak for the respiration rate is evident and the detected heartbeat rate (70 bpm) matches exactly the rate from the reference ECG (70 bpm as well).

C. Measurement Scenarios

To test the system under real conditions, the shown measurements were also taken under several different scenarios of target and radar positions. Two setups feature the PUT in an upright sitting position, measuring the vital signs from the front and

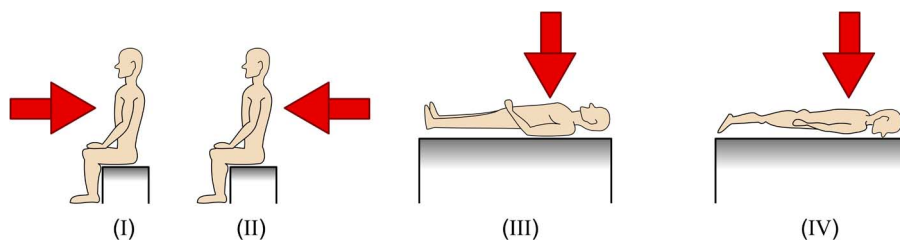


Fig. 12. Measurement positions of the PUT with direction of observation and position of the radar sensor marked as a red arrow.

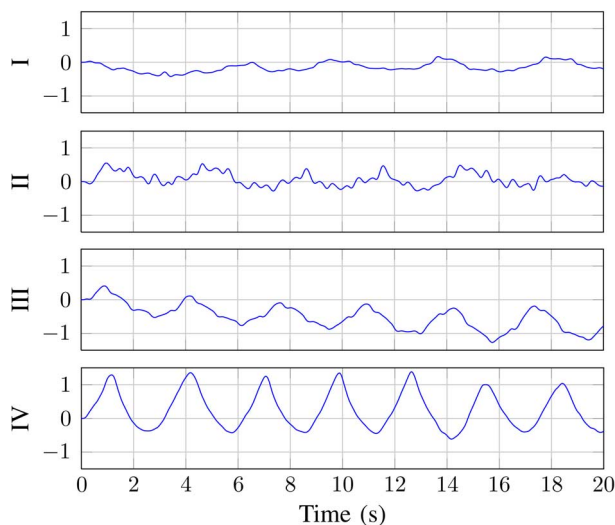


Fig. 13. Time-domain signals featuring the breathing process of low-pass-filtered raw data for different measurement scenarios according to Fig. 12. Vertical scaling is in millimeters.

the back of the patient. The other two scenarios were acquired, while the PUT was lying on his back and in the abdominal position, respectively. In this scenario, the radar sensor is positioned on a table over the patient at a distance of approximately 1 m. This setups are illustrated in Fig. 12.

As can be seen in Figs. 13 and 14, the results show excellent performance and detection accuracy in all test cases. Nevertheless, the heartbeat detection is more challenging when the PUT is in position IV, since the superimposed heartbeat signal is nearly negligible if compared with the amplitude of the respiration signal. Also, the time-dependant scaling of the amplitude is a result of the breathing influence and filtering. Nevertheless, the periodicity and the principle characteristics states accurate heartbeat detection. Excellent heartbeat detection can be performed when the PUT is monitored as in position II (PUT is in a seated position and is observed from the back). The detected heart rates are 66 bpm for position I, 68 bpm for position II, 69 bpm for position III, and 63 bpm for position IV. The difference between the detected heart rate for different positions is due to a faulty periodical peak detection mostly due to measurement nonidealities that influence the measurement. Longer detection times would allow a better signal detection with an FFT. These results lead to interesting conclusions for several monitoring applications where the PUT is not necessarily able to be monitored in a standard position. Results are comparable to measurements conducted with conventional CW radar sensors as can be

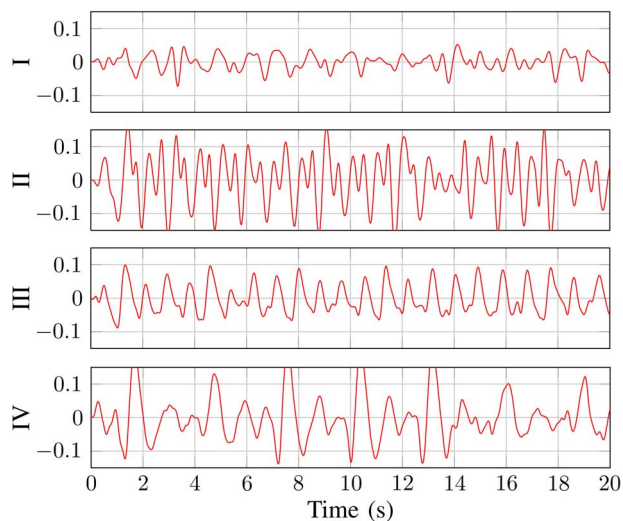


Fig. 14. Time-domain signals of bandpass-filtered heartbeat signal for different measurement scenarios according to Fig. 12. Vertical scaling is in millimeters.

observed in [13]. However, the proposed six-port-based radar sensor has additional advantages, due to better performance at higher operating frequencies and potentially higher spacial resolution and accuracy if compared with other traditional radar topologies at the same frequency of operation, as described in [20] and [32].

IX. CONCLUSION

A novel remote respiration and heartbeat monitoring sensor has been presented. The proposed device is based on the six-port interferometer radar principle working with a CW signal at 24 GHz with a very low-power microwave signal of less than 3 μ W. This technique features several advantages with respect to classical radar concepts. High accuracy in the micrometer scale as well as low system complexity are some of the benefits of the six-port receiver. A CW radar signal is sent towards the PUT to observe minor mechanical movements of the patient's body. These movements are caused by the respiration as well as heartbeat and can be tracked by analyzing the phase modulation of the backscattered signal.

Simple digital signal-processing algorithms allow a clear detection of the patient's respiration rate as well as heartbeat from the raw radar signal reflected from the person's torso. Different body areas have been observed by the proposed six-port radar to verify the system performance under different measurement scenarios. A PUT has been monitored from the front side of the torso as well as from the backside when lying on a bed

and when sitting on a chair. Measurements show excellent performance under all investigated conditions. The results confirm that the six-port receiver is suitable for accurate remote vital-sign monitoring.

REFERENCES

- [1] R. Pamphlett, J. Raisanen, and S. Kum-Jew, "Vertebral artery compression resulting from head movement: A possible cause of the sudden infant death syndrome," *Pediatrics*, vol. 103, no. 2, pp. 460–463, 1999.
- [2] C. Hunt and F. Hauck, "Sudden infant death syndrome," *Can. Med. Assoc. J.*, vol. 174, no. 13, pp. 1309–1310, 2006.
- [3] G. Data, "Cardiovascular monitoring and diagnostic devices—Global pipeline analysis, competitive landscape and market forecasts to 2017," Market Research.com, Jun. 2011, pp. 1–103.
- [4] C. Gu, C. Li, J. Lin, J. Long, J. Huangfu, and L. Ran, "Instrument-based noncontact doppler radar vital sign detection system using heterodyne digital quadrature demodulation architecture," *IEEE Trans. Instrum. Meas.*, vol. 59, no. 6, pp. 1580–1588, Jun. 2010.
- [5] J. Lin, "Microwave sensing of physiological movement and volume change: A review," *Bioelectromagn.*, vol. 13, no. 6, pp. 557–565, 1992.
- [6] N. Andre, S. Druart, P. Gerard, R. Pampin, L. Moreno-Hagelsieb, T. Kezai, L. Francis, D. Flandre, and J.-P. Raskin, "Miniaturized wireless sensing system for real-time breath activity recording," *IEEE Sensors J.*, vol. 10, no. 1, pp. 178–184, Jan. 2010.
- [7] K. Watanabe, T. Watanabe, H. Watanabe, H. Ando, T. Ishikawa, and K. Kobayashi, "Noninvasive measurement of heartbeat, respiration, snoring and body movements of a subject in bed via a pneumatic method," *IEEE Trans. Biomed. Eng.*, vol. 52, no. 12, pp. 2100–2107, Dec. 2005.
- [8] S.-G. Kim, H. Kim, Y. Lee, I.-S. Kho, and J.-G. Yook, "5.8 GHz vital signal sensing doppler radar using isolation-improved branch-line coupler," in *Proc. 3rd Eur. Radar Conf.*, Sep. 2006, pp. 249–252.
- [9] S. Ayhan, M. Pauli, T. Kayser, S. Scherr, and T. Zwick, "Fmcw radar system with additional phase evaluation for high accuracy range detection," in *Proc. Eur. Radar Conf.*, Oct. 2011, pp. 117–120.
- [10] S. Ayhan, P. Pahl, T. Kayser, M. Pauli, and T. Zwick, "Frequency estimation algorithm for an extended fmcw radar system with additional phase evaluation," in *Proc. German Microw. Conf.*, Mar. 2011, pp. 1–4.
- [11] S. Max, M. Vossiek, and P. Gulden, "Fusion of fmcw secondary radar signal beat frequency and phase estimations for high precision distance measurement," in *Proc. Eur. Radar Conf.*, Oct. 2008, pp. 124–127.
- [12] N. Pohl, T. Jaeschke, and K. Aufinger, "An ultra-wideband 80 GHz FMCW radar system using a SiGe bipolar transceiver chip stabilized by a fractional-n PLL synthesizer," *IEEE Trans. Microw. Theory Tech.*, vol. 60, no. 3, pp. 757–765, Mar. 2012.
- [13] J. H. Choi and D. K. Kim, "A remote compact sensor for the real-time monitoring of human heartbeat and respiration rate," *IEEE Trans. Biomed. Circuits Syst.*, vol. 3, no. 3, pp. 181–188, Jun. 2009.
- [14] G. Vinci, A. Koelpin, and R. Weigel, "Employing six-port technology for phase-measurement-based calibration of automotive radar," in *Proc. Asia-Pacific Singapore Microw. Conf.*, Dec. 2009, pp. 329–332.
- [15] B. Laemmle, G. Vinci, L. Maurer, R. Weigel, and A. Koelpin, "A 77-GHz SiGe integrated six-port receiver front-end for angle-of-arrival detection," *IEEE J. Solid-State Circuits*, vol. 47, no. 9, pp. 1966–1973, Sep. 2012.
- [16] B. Huyart, J.-J. Laurin, R. Bosisio, and D. Roscoe, "A direction-finding antenna system using an integrated six-port circuit," *IEEE Trans. Antennas Propag.*, vol. 43, no. 12, pp. 1508–1512, Dec. 1995.
- [17] G. Vinci, F. Barbon, R. Weigel, and A. Koelpin, "A 77 GHz direction of arrival detector system with SiGe integrated six-port receiver," in *Proc. Radio Wireless Week*, Santa Clara, CA, USA, 2012, accepted for publication.
- [18] F. Barbon, G. Vinci, S. Lindner, R. Weigel, and A. Koelpin, "A six-port interferometer based micrometer-accuracy displacement and vibration measurement radar," in *IEEE MTT-S Int. Microw. Symp. Dig.*, June 2012, pp. 1–3.
- [19] A. Koelpin, G. Vinci, B. Laemmle, S. Lindner, F. Barbon, and R. Weigel, "Six-port technology for traffic safety," *IEEE Microw. Mag.*, vol. 13, no. 3, pp. 118–127, Mar. 2012.
- [20] A. Stelzer, C. Diskus, K. Lubke, and H. Thim, "A microwave position sensor with submillimeter accuracy," *Microwave Theory and Techniques, IEEE Trans.*, vol. 47, no. 12, pp. 2621–2624, Dec. 1999.
- [21] E. Moldovan, S.-O. Tatu, T. Gaman, K. Wu, and R. Bosisio, "A new 94-GHz six-port collision-avoidance radar sensor," *IEEE Trans. Microw. Theory Tech.*, vol. 52, no. 3, pp. 751–759, Mar. 2004.

- [22] B. Boukari, E. Moldovan, S. Affes, K. Wu, R. Bosisio, and S. Tatu, "Six-port FMCW collision avoidance radar sensor configurations," in *Proc. Can. Conf. Electr. Comput. Eng.*, May 2008, pp. 305–308.
- [23] G. Engen and C. Hoer, "Application of an arbitrary 6-port junction to power-measurement problems," *IEEE Trans. Instrum. Meas.*, vol. IM-21, no. 4, pp. 470–474, Nov. 1972.
- [24] A. Koelpin, G. Vinci, B. Laemmle, D. Kissinger, and R. Weigel, "The six-port in modern society," *IEEE Microw. Mag.*, vol. 11, no. 7, pp. 35–43, Nov.–Dec. 2010.
- [25] G. Vinci, A. Koelpin, F. Barbon, and R. Weigel, "Six-port-based direction-of-arrival detection system," in *Proc. Asia-Pacific Microw. Conf.*, Dec. 2010, pp. 1817–1820.
- [26] F. M. Ghannouchi and A. Mohammadi, *The Six-Port Technique*. Norwood, MA, USA: Artech House, 2009.
- [27] F. Wooten, *Optical Properties of Solids*. New York: Academic, 1972.
- [28] S. Silberagl, *Taschenatlas der Physiologie*, 7th ed. Stuttgart, Germany: Thieme Georg Verlag, 2007, vol. 3.
- [29] S. Winter, H. Ehm, A. Koelpin, and R. Weigel, "Diode power detector dc operating point in six-port communications receivers," in *Proc. Eur. Microw. Conf.*, Oct. 2007, pp. 795–798.
- [30] F. Barbon, G. Vinci, S. Lindner, R. Weigel, and A. Koelpin, "Signal processing strategies for six-port based direction of arrival detector systems," in *Proc. Int. Multi-Conf. Syst., Signals Devices*, Chemnitz, Germany, accepted for publication.
- [31] I. Skyworks Solutions, Mixer and Detector Diodes ser. Application Note 200826 Rev. A, 2008.
- [32] G. Vinci, S. Lindner, F. Barbon, R. Weigel, and A. Koelpin, "Promise of a better position," *IEEE Microw. Mag.*, vol. 13, no. 7, pp. S41–S49, Nov.–Dec. 2012.



Gabor Vinci (S'06) was born in 1984. He received B.S. degree in microelectronics from the University of Padua, Padua, Italy, in 2005, and the M.S. degree in microwave engineering from the Technical University of Munich, Munich, Germany, in 2007, under the guidance of Prof. Russer. He is currently working toward the Ph.D. degree at the University of Erlangen-Nuremberg, Erlangen, Germany.

His thesis work was conducted at Daimler Research Center, Ulm, Germany, in the field of automotive antennas. He is currently a Research Assistant with the Institute for Electronics Engineering, University of Erlangen-Nuremberg, Erlangen, Germany. His research topics relate to innovative 24- and 77-GHz radar technology for automotive and industrial applications. He has worked on several industrial projects in different areas, particularly in antenna design, short-range high-resolution radar, as well as concept engineering and system design. Furthermore, he serves as a reviewer for several journals and conferences.

Mr. Vinci is a member of the IEEE Microwave Theory and Techniques Society (MTT-S).



Stefan Lindner (S'12) was born in Kulmbach, Germany, in 1985. He received the Diploma in mechatronics in 2011 at the University of Erlangen-Nuremberg, Erlangen, Germany, where he is currently working toward the Ph.D. degree.

Since 2012, he has been with the Institute for Electronics Engineering, University of Erlangen-Nuremberg, Erlangen, Germany. His research topics are related to innovative radar technology based on the six-port receiver. Primarily, he is working with system simulation, baseband design, as well as digital signal

processing.



Francesco Barbon (S'11) was born in Padua, Italy, in 1985. He received the B.S. degree from the Università degli Studi di Padova, Padua, Italy, in 2008, and the M.S. degree from the University of Erlangen-Nuremberg, Erlangen, Germany, in 2011, both in telecommunications.

He is currently a Research Assistant with the Institute for Electronics Engineering, University of Erlangen-Nuremberg, Erlangen, Germany, working on high-resolution industrial radar sensors based on the six-port interferometer technique. His main topics are signal conditioning and acquisitions.



Sebastian Mann (S'12) was born in Nuremberg, Germany, in 1987. He received the Diploma in electrical engineering from the University of Erlangen-Nuremberg, Erlangen, Germany, in 2012.

He is currently a Research Assistant with the Institute for Electronics Engineering, University of Erlangen-Nuremberg, Erlangen, Germany. He is involved with different industrial projects based on the six-port interferometer technique. His research interests are in the area of microwave circuits and components design. At present, he investigates on

high-precision 61-GHz radar sensors for industrial applications.



Maximilian Hofmann (S'09) was born in Coburg, Germany, in 1985. He received the Dipl.-Ing. degree in electrical, electronic and communications engineering from the University of Erlangen-Nuremberg, Erlangen, Germany, in 2010.

In 2010, he joined the Institute for Electronics Engineering, University of Erlangen-Nuremberg, Erlangen, Germany, as a Research Assistant. His research interests include RF and millimeter-wave sensor circuits for biomedical applications.

Mr. Hofmann is a member of the IEEE Microwave Theory and Techniques Society (IEEE MTT-S), the IEEE Engineering in Medicine and Biology Society, and the German Association for Electrical, Electronic and Information Technologies (VDE). He received the First Prize at the IEEE Biomedical Wireless Technologies (BioWireless) Student Paper Competition, Santa Clara, CA, in 2012.



Alexander Duda was born in Wuerzburg, Germany, in 1988. He is currently working toward the B.S. degree in medical engineering at the University of Erlangen-Nuremberg, Erlangen, Germany.

His research focuses on vital-sign monitoring based on six-port radar measurements.



Robert Weigel (S'88–M'89–SM'95–F'02) was born in Ebermannstadt, Germany, in 1956. He received the Dr.-Ing. and Dr.-Ing.habil. degrees in electrical engineering and computer science from the Munich University of Technology, Munich, Germany, in 1989 and 1992, respectively.

From 1982 to 1988, he was a Research Engineer, from 1988 to 1994, a Senior Research Engineer, and from 1994 to 1996, a Professor of RF circuits and systems with the Munich University of Technology, Munich, Germany. In the winter of 1994/1995, he was a

Guest Professor of SAW technology with the Vienna University of Technology, Vienna, Austria. From 1996 to 2002, he was Director of the Institute for Communications and Information Engineering, University of Linz, Linz, Austria. In August 1999, he cofounded DICE—Danube Integrated Circuit Engineering, Linz, Austria, meanwhile an Infineon Technologies Design Center (DICE) and an Intel company (DMCE) which are devoted to the design of, respectively, industrial electronics and mobile radio electronics. In 2000, he has been appointed a Professor for RF engineering at Tongji University, Shanghai, China. Also in 2000, he cofounded the Linz Center of Competence in Mechatronics. Since 2002, he has been head of the Institute for Electronics Engineering, University of Erlangen-Nuremberg, Erlangen, Germany. In 2009 and 2012, respectively, he cofounded eesy-id, Erlangen, and eesy-ic, Nuremberg, Germany, both dealing with electronics engineering. He has been engaged in the research and development of microwave theory and techniques, integrated optics, high-temperature superconductivity, SAW technology, digital and microwave communication systems, and automotive EMC. In these fields, he has authored and coauthored more than 700 papers and given about 300 international presentations. His review work includes European and Asian research projects and international journals.

Dr. Weigel is a member of the Institute for Components and Systems of The Electromagnetics Academy, the German ITG, and the Austrian VE. He serves on several editorial boards and advisory boards. He is an elected scientific advisor of the German Research Foundation. Within the IEEE Microwave Theory and Techniques Society (IEEE MTT-S), he has been Founder and Chair of the Austrian COM/MTT Joint Chapter, Region 8 Coordinator and, during 2001 to 2003 Distinguished Microwave Lecturer. He is an AdCom Member and Chair of MTT-2 Microwave Acoustics. In 2002, he received the German ITG Award and in 2007 the IEEE Microwave Applications Award.



Alexander Koelpin (S'04–M'10) received the Diploma in electrical engineering and Ph.D. degree from the University of Erlangen-Nuremberg, Erlangen, Germany, in 2005 and 2010, respectively. Currently he is working towards his *venia legendi*.

Since 2005, he has been with the Institute for Electronics Engineering, Friedrich-Alexander University of Erlangen-Nuremberg, Erlangen, Germany, and, since 2007, been team leader of Circuits, Systems and Hardware Test. His research interests are in the areas of microwave circuits and systems, wireless

communication systems, local positioning, and six-port technology. He has authored or coauthored over 50 publications in his areas of interest.

Dr. Koelpin he received the IEEE COM innovation award in 2005. Furthermore, he serves as a reviewer for several journals and conferences and is member of the IEEE Microwave Theory and Techniques Society (IEEE MTT-S) technical committee MTT-16.